Theoretical and Applied Climatology (2021) 145:345–361
https://doi.org/10.1007/s00704-021-03639-4

ORIGINAL PAPER

Evaluating spatial patterns of Asian meteorological drought variations and associated SST anomalies in CMIP6 models

Yanting Zhang [1,2] · Renguang Wu [3,1,4,5]

Received: 10 December 2020 / Accepted: 27 April 2021 / Published online: 4 May 2021

Abstract

This study evaluates the spatial patterns of the Asian summer drought variations and the associated sea surface temperature (SST) anomalies in 42 Coupled Model Intercomparison Project (CMIP6) models during 1950–2014. The analysis is focused on the meteorological drought measured using the standardized precipitation index (SPI). The evaluation is conducted for short-term, medium-term, and long-term droughts represented by 3-month, 9-month, and 24-month SPI, respectively. Most of the 42 models are able to capture the observed leading spatial pattern of short-term and medium-term drought variations, characterized by a north-south dipole structure. In contrast, most models fail to simulate the observed leading spatial pattern of long-term drought variations, featuring a southwest-northeast oriented tripole distribution. Further analysis shows that most models can represent the spatial pattern of interannual variation of long-term drought with a north-south dipole structure, but cannot produce the spatial pattern of interdecadal variation and trend of long-term drought. In most of the models, the dipole pattern of short-term and medium-term drought variations is associated with an El Niño–type SST anomaly pattern in the tropical Indo-Pacific region, which is similar to the observations, so is the dipole pattern of interannual variation of long-term droughts. This is attributed to the ability of most models to capture the tropica Indo-Pacific SST-related large-scale atmospheric circulation anomaly pattern.

1 Introduction

Droughts are among the major nature hazards and can induce large damages in agriculture, ecosystem, and socioeconomics (Wilhite 2000). Droughts affect more people than any other types of natural disasters (Zargar et al. 2011). Understanding the drought changes is a basis for improving the prediction of occurrence of droughts and mitigating the adverse consequences of droughts. Thus, efforts have been made in the past to understand the changes of droughts (Dai 2011; Huang et al. 2008, 2012; Trenberth et al. 2014; Zhang and Zhou 2015; Guan et al. 2017).

Climate models have been widely employed to investigate the historical and future changes of droughts (Sheffield and Wood 2008; Kim and Byun 2009; Dai 2013; Orlowsky and Seneviratne 2013; Touma et al. 2015; Zhao and Dai 2015; Huang et al. 2017b; Lehner et al. 2017; Su et al. 2018). Discrepancies in drought changes are identified between models and the observations (Ault et al. 2012; Sheffield et al. 2012; Damberg and AghaKouchak 2014; Trenberth et al. 2014), which is, to large part, related to the deficiency in the model physics (Orlowsky and Seneviratne 2013). Large spread and uncertainty are often encountered in the model projected future changes of droughts (Orlowsky and Seneviratne 2013; Prudhomme et al. 2014; Ukkola et al. 2018; Wu et al. 2020). Thus, it remains to be investigated how the climate models perform in capturing the characteristics of drought changes (Huang et al. 2016).

Studies have been conducted to evaluate climate models in historical drought simulations (Sheffield et al. 2012; Orlowsky and Seneviratne 2013; Nasrollahi et al. 2015; Ukkola et al. 2018). Sheffield et al. (2012) identified several regions with significant increasing trends of droughts

✉ Renguang Wu
renguang@zju.edu.cn

[1] Center for Monsoon System Research, Institute of Atmospheric Physics, Chinese Academy of Sciences, Beijing, China

[2] College of Earth and Planetary Sciences, University of Chinese Academy of Sciences, Beijing, China

[3] School of Earth Sciences, Zhejiang University, Hangzhou 310027, China

[4] State Key Laboratory of Numerical Modeling for Atmospheric Sciences and Geophysical Fluid Dynamics, Institute of Atmospheric Physics, Chinese Academy of Sciences, Beijing, China

[5] Southern Marine Science and Engineering Guangdong Laboratory (Zhuhai), Zhuhai, China

measured using the Palmer Drought Severity Index (PDSI) during 1950–2008. Orlowsky and Seneviratne (2013) analyzed drought changes based on the standardized precipitation index (SPI) during 1901–2005 in both the observations and the fifth phase of the Coupled Model Intercomparison Project (CMIP5) models and found large uncertainty in regional drought trends. Nasrollahi et al. (2015) compared the area of drought based on SPI in the CMIP5 multimodel ensemble simulations against the ground-based observations. They found that the models agree generally with the observations at the global and hemispheric scale, but disagree with the observations in regional drying and wetting trends. Ukkola et al. (2018) analyzed several drought metrics in 20 CMIP5 model historical simulations during 1951–2004 and found that the models had large discrepancies at the regional scale. In particular, the models underestimate the intensity of precipitation-related drought.

Previous studies mostly focus on analyzing trends or long-term changes of droughts. As precipitation changes occur on different time scales, it is essential to evaluate the drought variations on various time scales in the models compared to the corresponding observations. Severe droughts often occur in certain areas with devastating regional consequences (Lewis et al. 2011; Barriopedro et al. 2012; McGrath et al. 2012; Orlowsky and Seneviratne 2012; Peterson et al. 2012). Thus, it is valuable to assess whether the spatial patterns of historical drought variations on different time scales can be captured by the models. Such assessment provides information to what extent the factors and processes of drought variations are represented properly in the climate models, which is a basis for projection of future drought changes using climate models. The occurrence of drought is induced by external forcing, such as sea surface temperature (SST) anomalies, which plays a vital role in climate change (Guan et al. 2015a, 2019). It is important to know whether the occurrence of droughts in the models is linked to specific SST anomaly patterns as in the observations. This is relevant to whether the factors of drought variations are realistic in the models.

The present study evaluates the spatial patterns of drought variations on different time scales and the associated SST and atmospheric circulation anomalies in climate models. The focus of the analysis is the Asian region that contains about 67% of the world's population (Guan et al. 2015b) and include large arid and semi-arid regions (White and Nackoney 2003), which makes it vulnerable to drought-related disasters (Zhang et al. 2017). Droughts can be assessed from different aspects, including meteorological, hydrological, and agricultural. This study focuses on meteorological droughts estimated using the SPI. Changes in droughts may depend upon the indices of drought (Burke and Brown 2008; Sheffield et al. 2012; Taylor et al. 2012; Dai 2013). We assess the variations of short-term, medium-term, and long-term droughts represented by 3-month, 9-month, and 24-month SPI, respectively. SPI is a widely used index of meteorological drought that is based on accumulated precipitation over a certain length of time period (McKee et al. 1993) and has several advantages over several other drought indices (Hayes et al. 2011). We concentrate on boreal summer (June–July–August, JJA) mean SPI indices. The goal of this study is to identify whether the models have deficiency in the simulations of spatial patterns of meteorological drought variations on different time scales. This serves to illustrate whether the models are suitable to be used for projection of future meteorological drought changes.

The organization of the rest of the paper is as follows. In Section 2, we describe the data of the observations and models as well as the methods. In Section 3, we evaluate the spatial patterns of short-term, medium-term, and long-term drought variations, respectively. In Section 4, we compare the SST and atmospheric circulation anomalies corresponding to the interannual variations of short-term, medium-term, and long-term droughts, respectively. Summary is provided in Section 5 along with discussions.

2 Data and methods

The present study uses monthly precipitation from the Climatic Research Unit Time Series (CRU TS) version 4.03 (Harris et al. 2014). The CRU TS version 4.03 precipitation data have a horizontal resolution of 0.5°×0.5° and span the time period 1901–2018, which were downloaded from https://crudata.uea.ac.uk/cru/data/precip/. Monthly mean SST is from the Extended Reconstruction of Sea Surface Temperature version 5 (ERSST5) (Huang et al. 2017a). The ERSST5 SST has a spatial resolution of 2°×2° and is available from 1854 to present. The ERSST5 SST data were obtained through https://www1.ncdc.noaa.gov/pub/data/cmb/ersst/v5/.

We use monthly precipitation data from the historical simulations of 42 Coupled Model Intercomparison Project (CMIP6) models that participated the sixth Assessment Report (AR6) of Intergovernmental Panel on Climate Change (IPCC) (Eyring et al. 2016). Among those 42 models, 35 models provide monthly mean SST. The model data cover the time period 1850–2014. Only the first ensemble member of each model simulations is used in this analysis. The names, institutions, and spatial resolutions of those models are listed in Table 1. The CMIP6 model outputs were downloaded from https://esgf-node.llnl.gov/search/cmip6/.

The present study uses SPI (McKee et al. 1993) as a measure of meteorological drought. Our focus is on drought variations related to regional atmospheric circulation. This differs from other drought indices that include temperature. SPI is calculated using monthly precipitation in the observations and individual model simulations. We calculate SPI03,

Table 1 List of information of CMIP6 models used in the study.

	Model name	Modeling Center	Resolution (latitude× longitude)	
			PR(42)	SST(35)
1	ACCESS-CM2	Australian Research Council Centre of Excellence for Climate System Science, Australia	144×192	300×360
2	ACCESS-ESM1-5	Commonwealth Scientific and Industrial Research Organisation, Australia	145×192	300×360
3	AWI-CM-1-1-MR	Alfred Wegener Institute, Germany	192×384	830305 (unstructured)
4	AWI-ESM-1-1-LR	Alfred Wegener Institute, Germany	96×192	126859 (unstructured)
5	BCC-CSM2-MR	Beijing Climate Center, China	160×320	232×360
6	BCC-ESM1	Beijing Climate Center, China	64×128	232×360
7	CAMS-CSM1-0	Chinese Academy of Meteorological Sciences, China	160×320	200×360
8	CanESM5	Canadian Centre for Climate Modelling and Analysis, Canada	64×128	291×360
9	CAS-ESM2-0	Chinese Academy of Sciences, China	128×256	196×360
10	CESM2	NCAR, Climate and Global Dynamics Laboratory, USA	192×288	384×320
11	CESM2-FV2	NCAR, Climate and Global Dynamics Laboratory, USA	96×144	384×320
12	CESM2-WACCM	NCAR, Climate and Global Dynamics Laboratory, USA	192×288	384×320
13	CESM2-WACCM-FV2	NCAR, Climate and Global Dynamics Laboratory, USA	96×144	384×320
14	CIESM	Tsinghua University, China	192×288	384×320
15	E3SM-1-0	Energy Exascale Earth System Model project, USA	180×360	
16	E3SM-1-1	Energy Exascale Earth System Model project, USA	180×360	
17	E3SM-1-1-ECA	Energy Exascale Earth System Model project, USA	180×360	
18	EC-Earth3	EC-Earth-Consortium	256×512	292×362
19	EC-Earth3-Veg	EC-Earth-Consortium	256×512	292×362
20	EC-Earth3-Veg-LR	EC-Earth-Consortium	160×320	292×362
21	FGOALS-f3-L	Chinese Academy of Sciences, China	180×288	218×360
22	FGOALS-g3	Chinese Academy of Sciences, China	80×180	218×360
23	FIO-ESM-2-0	First Institute of Oceanography, China	192×288	384×320
24	GFDL-ESM4	NOAA Geophysical Fluid Dynamics Laboratory, USA	180×288	180×360
25	GISS-E2-1-G	NASA Goddard Institute for Space Studies, USA	90×144	90×144
26	GISS-E2-1-H	NASA Goddard Institute for Space Studies, USA	90×144	90×144
27	INM-CM4-8	Institute for Numerical Mathematics, Russia	120×180	
28	INM-CM5-0	Institute for Numerical Mathematics, Russia	120×180	
29	IPSL-CM6-LR	Institut Pierre Simon Laplace, France	143×144	332×362
30	KACE-1-0-G	National Institute of Meteorological Sciences, Republic of Korea	144×192	
31	MCM-UA-1-0	University of Arizona, USA	80×96	80×192
32	MIROC6	MIROC, Japan	128×256	256×360
33	MPI-ESM-1-2-HAM	HAMMOZ-Consortium	96×192	220×256
34	MPI-ESM1-2-HR	Max Planck Institute for Meteorology, Germany	192×384	404×802
35	MPI-ESM1-2-LR	Max Planck Institute for Meteorology, Germany	96×192	220×256
36	MRI-ESM2-0	Meteorological Research Institute, Japan	160×320	363×360
37	NESM3	Nanjing University of Information Science and Technology, China	96×192	292×362
38	NorCPM1	Norwegian Climate Centre, Norway	96×144	384×320
39	NorESM2-LM	Norwegian Climate Centre, Norway	96×144	385×360
40	NorESM2-MM	Norwegian Climate Centre, Norway	192×288	385×360
41	SAM0-UNICON	Seoul National University, Republic of Korea	192×288	384×320
42	TaiESM1	Academia Sinica, Taiwan	192×288	

SPI09, and SPI24 to represent short-term, medium-term, and long-term drought, respectively. The SPI is derived as follows. First, a time series is constructed by averaging the precipitation over a given time period (e.g., 3 months for SPI03) by starting backward from the current time. Then, the time series is transformed to a normal distribution function. Next, the SPI values are determined from the transformed time series. For details of the method calculating different SPIs, refer to Lopes-Moreno and Vicente-Serrano (2008). After obtaining monthly SPI values, we construct JJA mean SPIs, which are used in the present analysis.

An empirical orthogonal function (EOF) analysis is employed to extract the leading spatial patterns and the corresponding principal component (PC) time series of short-term, medium-term, and long-term drought variations in JJA. Both the model and observed SPIs are interpolated to the resolution of 1°×1° using a bilinear interpolation method before conducting the EOF analysis. Regression analysis with respect to the PC time series is utilized to obtain the spatial distribution of anomalies corresponding to the EOF modes. The Student *t* test is used to estimate the level of the statistical significance of correlation coefficient. The least-square linear regression method is applied to a time series to obtain the corresponding linear trend. An 11-year weighted running mean using the Lanczos filter weights is applied to the detrended time series to obtain the interdecadal variation. The interannual variation is derived by removing the linear trend and interdecal variation from the original time series. The percent variance of a time series accounted for by interannual component, interdecadal component, and linear trend is estimated by the ratio of the variance of the respective component versus the total variance. The time period of the present analysis is 1950–2014.

3 Spatial patterns and temporal components of drought variations

We start with an EOF analysis of JJA SPI03, SPI09, and SPI24 variations in both the observations and 42 individual CMIP6 model simulations over the domain of 20°–50°N and 60°–120°E for the time period 1950–2014. Figure 1(a–c) show JJA SPI03, SPI09, and SPI24 anomalies obtained by regression onto the PCs corresponding to EOF1 in the observations. The spatial pattern of the leading mode of JJA SPI03 and SPI09 variations displays a north-south dipole distribution across approximately 30°N (Fig. 1(a, b)). The spatial pattern of the leading mode of JJA SPI24 shows a southwest-northeast oriented tripole distribution (Fig. 1(c)).

To examine whether the CMIP6 models capture the leading modes in the observations, we calculate the spatial pattern correlation coefficient (PCC) between the observed SPI anomalies of the leading mode and the model SPI anomalies corresponding to the first two modes over the domain of 5°–60°N and 50°–150°E. Here, we focus on the modes in the models that are most similar to the leading mode in the observations, measured by the PCC value. Thus, we display the PCC in Fig. 2 for either the first or second mode in the 42 models. In most of the models, the leading mode of SPI03 and SPI09 resembles the leading mode in the observations with the PCC above 0.5 in majority of the models (Fig. 2(a, b)). This indicates that the dipole mode of short-term and medium-term variations is captured as a leading mode in most of the 42 models. In a few models (5 model for SPI03 and 7 model for SPI09), the second mode has a higher PCC value than the first mode with the observed leading mode. This indicates that these models do not produce the observed dipole pattern of short-term and medium-term drought variations as the first mode. In the following, we focus on the dipole EOF mode in the models. In 12 of the 42 models, the second mode of SPI24 has a higher PCC value than the first mode with the observed leading mode (Fig. 2(c)). About half of the models has a PCC value below 0.5, smaller than that for SPI03 and SPI09. This indicates that the models have a lower ability to capture the tripole mode of the long-term drought variations.

Based on the PCC values, we construct an ensemble mean of the dipole mode in the 42 CMIP6 models by averaging the JJA SPI03 and SPI09 anomalies corresponding to the first or second modes with a higher PCC. In a similar manner, we constructed an ensemble mean of the tripole mode in the models by averaging the JJA SPI24 anomalies corresponding to the first or second modes with a higher PCC. The results are displayed in Fig. 1(d–f). The dipole mode of SPI03 and SPI09 variations in the model ensemble mean is very similar to the corresponding observations (Fig. 1(a, d; b, e)). The tripole mode of SPI24 variations in the model ensemble mean, however, deviates from the corresponding observations with smaller positive anomalies over North China and Mongolia and opposite anomalies over the eastern Indochina Peninsula and the Philippines (Fig. 1(c, f)).

Inspection of the PC time series reveals another feature. The dipole mode of JJA SPI03 and SPI09 variations in the models are dominated by interannual variations as in the observations. This is illustrated in Fig. 3 that displays the percent variance accounted for by interannual component, interdecadal component, and linear trend during the analysis time period. The percent variance explained by the interannual component of the dipole mode of JJA SPI03 and SPI09 variations exceeds 75% in majority of the models, which is similar to the observations (Fig. 3(a, b)). The tripole mode of JJA SPI24 variations has a larger contribution from the interannual component in most of the models as well (Fig. 3(c)) but with a smaller percent variance compared to the dipole mode of JJA SPI03 and SPI09 variations. In many models, the contributions of interdecadal component and linear trend are important for JJA SPI24 variations, consistent with the observations

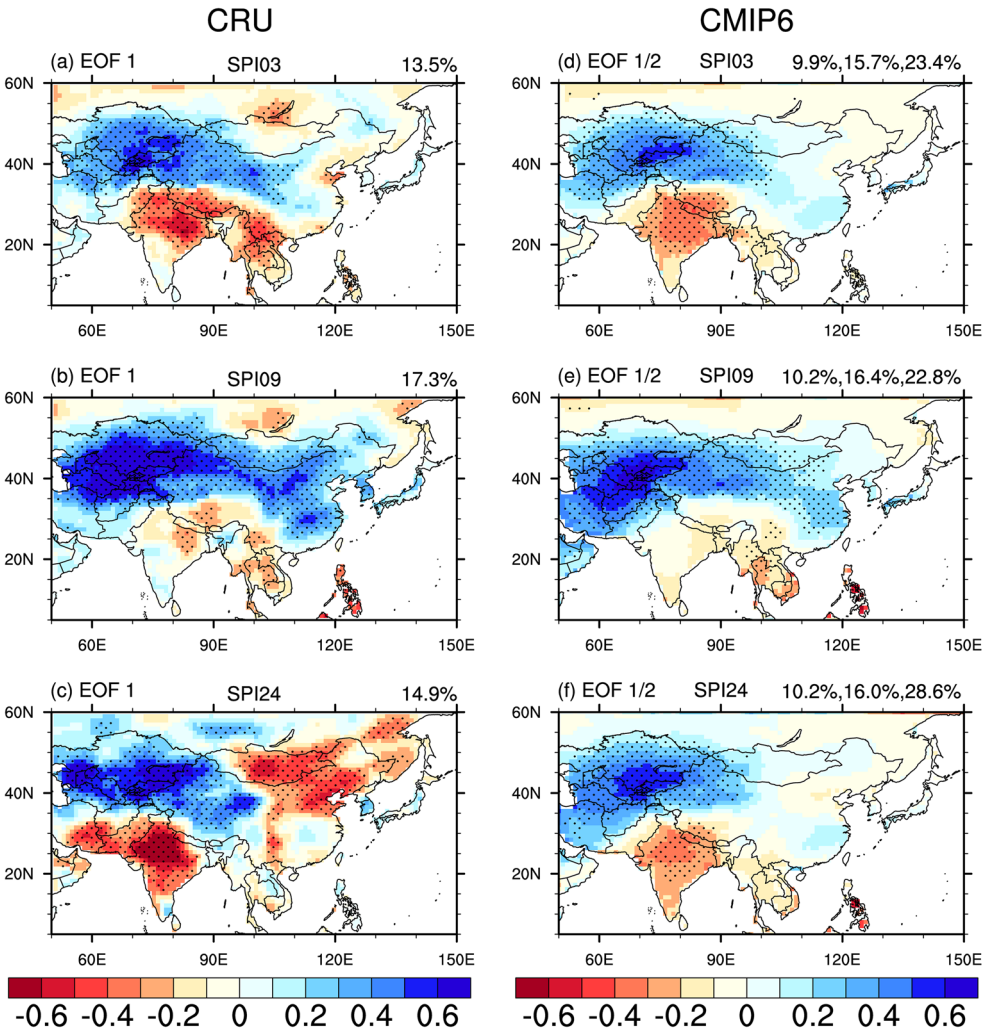

Fig. 1 The spatial pattern of the first EOF mode of JJA (**a**) SPI03, (**b**) SPI09, and (**c**) SPI24 variations based on the CRU precipitation data during 1950–2014. Stippling denotes grid points with statistically significant anomalies at the 95% confidence level. The number in the top right denotes the percent variance of the first EOF mode. Ensemble mean of the model spatial pattern of JJA (**d**) SPI03, (**e**) SPI09, and (**f**) SPI24 variations obtained by averaging the spatial patterns of the first or second EOF mode with the higher spatial pattern correlation coefficient with the observed spatial pattern of the first EOF mode during 1950–2014. Stippling denotes grid points where 80% or more of the 42 models have the same sign anomalies. The numbers in the top right denote the lowest, mean, and highest percent variances among the 42 first or second EOF modes. (**a**)–(**c**) are modified from Zhang and Wu (2021)

(Fig. 3(c)). The dominance of interannual component in the dipole mode of SPI03 and SPI09 variations indicates weak interdecadal changes and linear trends in regional spatial patterns of short-term and medium-term droughts, which agrees with previous studies. Orlowsky and Seneviratne (2013) found that regional droughts as measured by SPI03 and SPI12 display hardly any trends over the last decades in the observations and CMIP5 models. Nasrollahi et al. (2015) obtained that many regions do not show significant drying or wetting trends in the CMIP5 models and CRU precipitation data.

We perform a further EOF analysis for the three components of JJA SPI24 variations. In the observations, the leading mode of the interannual component of JJA SPI24 variations is a dipole pattern (Fig. 4(a)), similar to those of JJA SPI03 and SPI09 (Fig. 1(a, b)). The leading mode of the interdecadal component of JJA SPI24 variations is a tripole pattern (Fig. 4(b)), similar to that of the total JJA SPI24 variation (Fig. 1(c)). The distribution of the linear trend of JJA SPI24 displays regional features (Fig. 4(c)).

We calculate the PCC of the spatial distribution of three components of JJA SPI24 anomalies in individual models against the corresponding leading modes in the observations. It turns out that the leading mode of the interannual component of SPI24 variations in the observations is captured as a leading mode in 39 of the 42 models and as a second mode in 3 of the 42 models with the PCC values above 0.5 in most of the models (Fig. 5(a)). The tripole mode of the interdecadal component of SPI24 variations in the observations, however, is not reproduced in the models as indicated by the low PCC values below 0.3 in majority of the models (Fig. 5(b)). Similarly, the linear trend of SPI24 in the models differs from that in the observations with the PCC values below 0.3 in most models (Fig. 5(c)).

The ensemble mean of the dipole mode of interannual component of JJA SPI24 variations in the models constructed based on the PCC values (Fig. 4(d)) is quite similar to the corresponding observations (Fig. 4(a)). The ensemble mean of the tripole mode of interdecadal component of JJA SPI24 variations, however, is very weak though the spatial

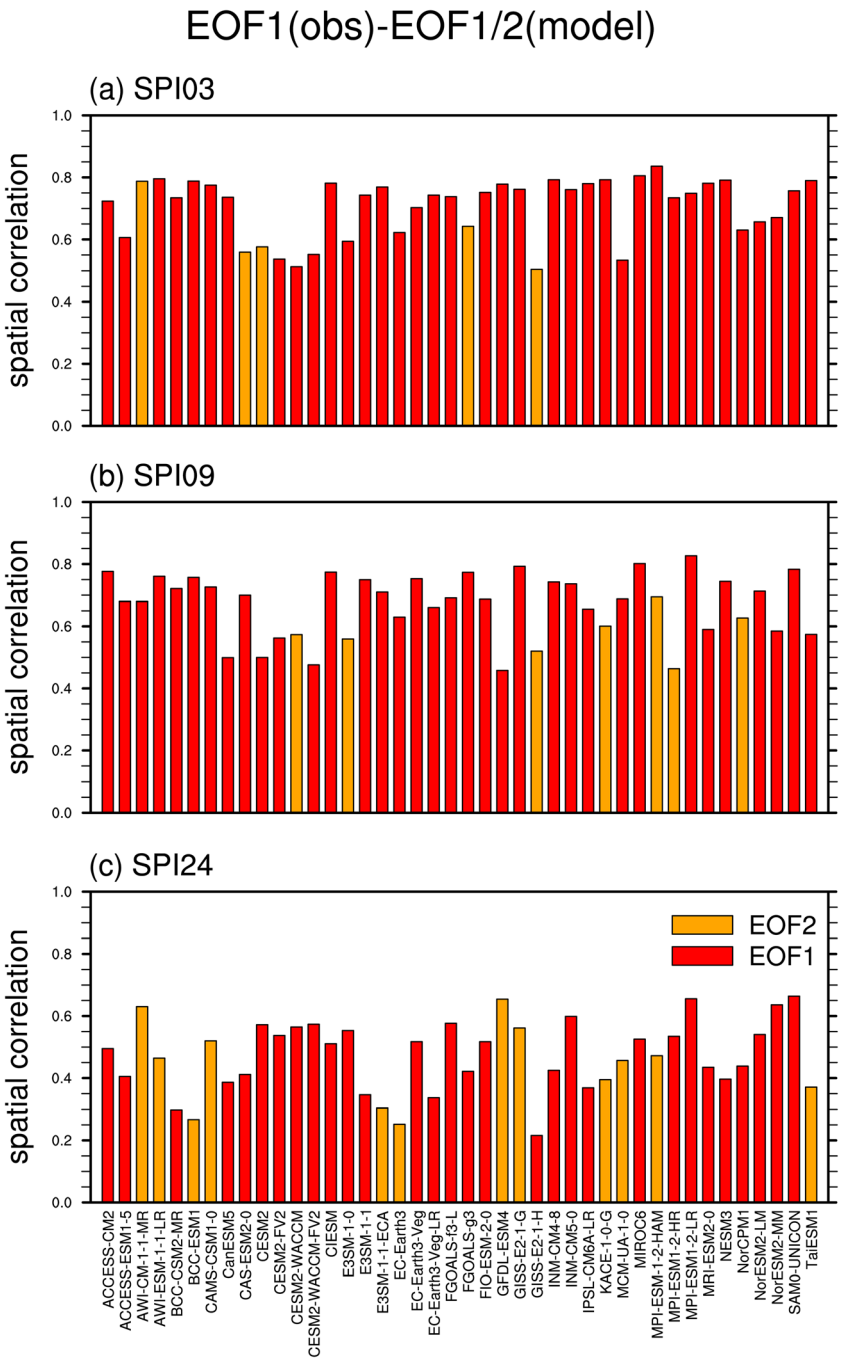

Fig. 2 The spatial pattern correlation coefficient of the spatial pattern of the first (red) or second (orange) EOF mode in the models with the observed spatial pattern of the first EOF mode of JJA (**a**) SPI03, (**b**) SPI09, and (**c**) SPI24 variations

distribution is similar to the corresponding observations (Fig. 4(e, b)). This indicates that there is likely a large spread in the spatial pattern of interdecadal variations of long-term droughts. The ensemble mean of the linear trend of JJA SPI24 (Fig. 4(f)) deviates largely from the observations (Fig. 4(c)). Positive trend is seen over southern China and negative trend covers the western China and the mid-latitude regions (Fig. 4(f)). The above results suggest that the models have difficulty to reproduce the interdecadal variations and trends of long-term droughts.

The difference in the trends of long-term droughts between the observations and model simulations is further illustrated in Fig. 6. In the observations, the first PC time series of the tripole pattern of JJA SPI24 displays an upward trend, which is significant at the 95% confidence level, with superposed interdecadal variations during the analysis period. The ensemble mean of the PC time series in the models does not show any trend. In addition, there is a large spread of the PC time series among the models. The fluctuations of the observed PC time series appear to be within the model spread. This result is

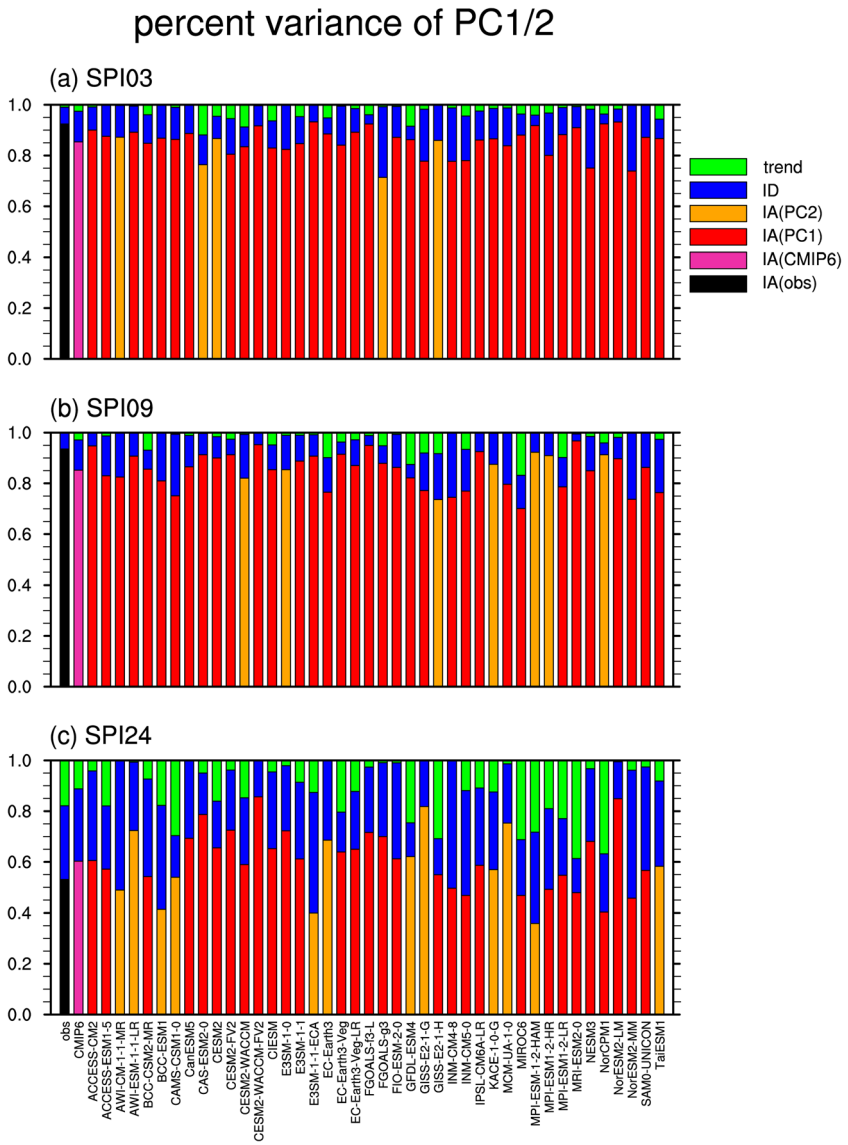

Fig. 3 The percent variance of interannual component (black for the observations, pink for the ensemble mean of CMIP6 models, red or orange for individual models), interdecadal component (blue), and linear trend (green) of the first (red) or second (orange) PC time series of JJA (**a**) SPI03, (**b**) SPI09, and (**c**) SPI24 variations

consistent with results of previous studies using the CMIP5 models that most models do not agree with each other and with the observations in regional drying and wetting trends (Orlowsky and Seneviratne 2013; Nasrollahi et al. 2015; Ukkola et al. 2018).

4 SST and atmospheric circulation anomalies for leading spatial patterns of drought variations

An important factor for the drought variations is SST anomalies. In this section, we examine whether the models reproduce the large-scale SST anomaly pattern corresponding to the dipole pattern of the interannual JJA SPI03, SPI09, and SPI24 variations. This provides information about the factors of drought variations in the models against the observations. Our analysis covers SST anomalies from preceding December–January–February (DJF) to JJA for JJA SPI03 and SPI09 variations and from DJF of the preceding year (denoted as DJF(-1)) to JJA for JJA SPI24 variations. In view of the persistence of the obtained SST anomalies, in the following, we only present SST anomalies in May–June–July (MJJ) for JJA SPI03, DJF and March–April–May (MAM) for JJA SPI09, and JJA in the preceding year (denoted as JJA(-1)) and preceding DJF for JJA SPI24, respectively. The selection of the above seasons is based on the time periods of precipitation used to calculate the JJA SPI03, SPI09, and SPI24.

In the observations, the tropical Indo-Pacific SST anomalies in MJJ corresponding to the dipole mode of JJA SPI03 variations display an El Niño–type distribution with positive SST anomalies in the equatorial central-eastern Pacific and tropical Indian Ocean and negative SST anomalies extending

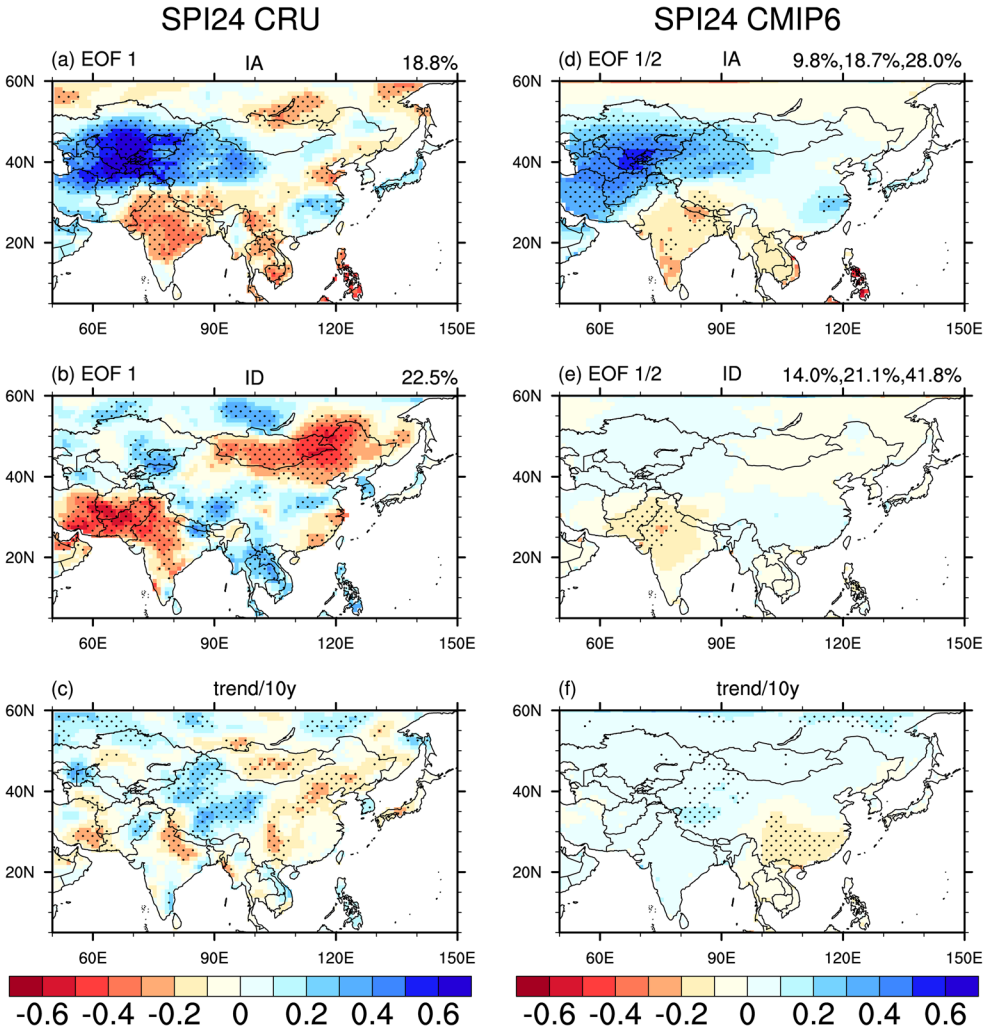

Fig. 4 The spatial pattern of the first EOF mode of (**a**) interannual component and (**b**) interdecadal component of JJA SPI 24 variations based on the CRU precipitation data during 1950–2014. Stippling denotes grid points with statistically significant anomalies at the 95% confidence level. The number in the top right denotes the percent variance of the first EOF mode. (**c**) The spatial pattern of the linear trend of JJA SPI 24 variations based on the CRU precipitation data during 1950–2014. Stippling denotes grid points with statistically significant trends at the 95% confidence level. Ensemble mean of the model spatial pattern of (**d**) interannual component and (**e**) interdecadal component of JJA SPI24 variations obtained by averaging the spatial patterns of the first or second EOF mode with the higher spatial pattern correlation coefficient with the observed spatial pattern of the first EOF mode during 1950-2014. Stippling denotes grid points where 80% or more of the 42 models have the same sign anomalies. The numbers in the top right denote the lowest, mean, and highest percent variances among the 42 first or second EOF modes. (**f**) Ensemble mean of the model linear trends of JJA SPI24 variations. Stippling denotes grid points where 80% or more of the 42 models have the same sign trends. (**a**)–(**c**) are modified from Zhang and Wu (2021)

northeastward and southeastward from the tropical western Pacific (Fig. 7(a)). The North Atlantic SST anomalies in MJJ show a tripole pattern with positive SST anomalies in the tropics and western middle latitudes and negative SST anomalies in the subtropics (Fig. 7(a)).

For evaluation of the short-term drought-related SST anomalies in the models, we first obtain the model simulated SST anomalies in MJJ corresponding to the dipole mode of interannual JJA SPI03 variations by regression with respect to the corresponding PC time series corresponding. Then, we calculate the PCC between the observed SST anomalies and the model simulated SST anomalies in MJJ for the tropical Indo-Pacific domain (30°S–30°N, 40°E–80°W) and the North Atlantic domain (0°–60°N, 70°W–0°), respectively. Most of the models capture reasonably the El Niño–type SST anomalies in the tropical Indo-Pacific region with the PCC values above 0.4 (Fig. 8(a)). About one-third of the models produce a tripole SST anomaly pattern in the North Atlantic region with the PCC values above 0.4 (Fig. 8(b)). There are five models with negative PCC values for the North Atlantic domain. Inspection of the SST anomalies in those five models reveals very different distribution of SST anomalies in the North Atlantic Ocean compared to the observations. In particular, in the NorESM2-LM, the SST anomalies in the tropical and middle latitude Atlantic Ocean tend to be opposite to the observations (not shown).

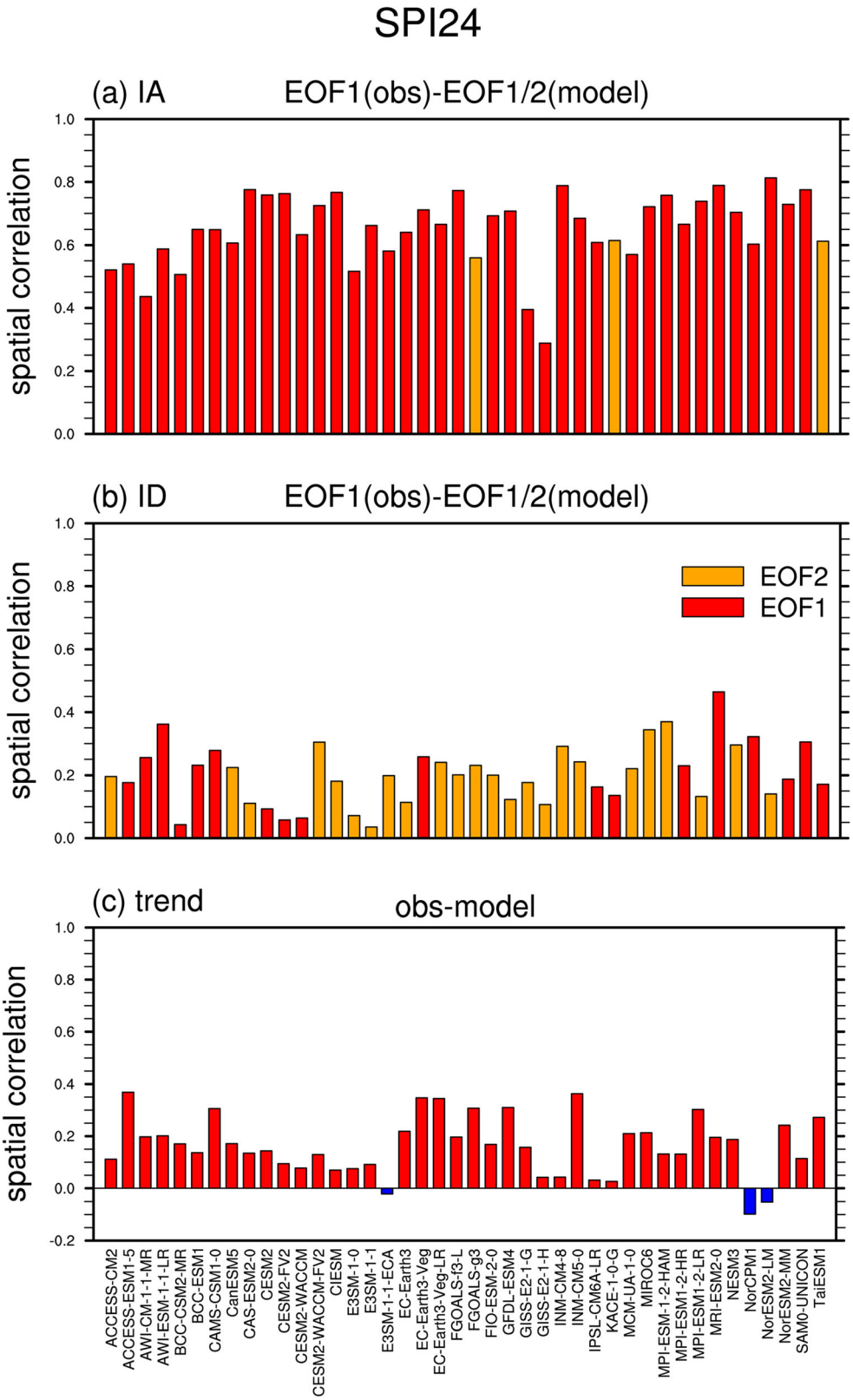

Fig. 5 The spatial pattern correlation coefficient of the spatial pattern of the first (red) or second (orange) EOF mode in the models with the observed spatial pattern of the first EOF mode of (**a**) interannual component and (**b**) interdecadal component of JJA SPI24 variations. (**c**) The spatial pattern correlation coefficient of the linear trends in the models with the observed linear trends of JJA SPI24 variations

The ensemble mean SST anomalies in the models, obtained by averaging the regressed SST anomalies associated with the dipole mode of interannual JJA SPI03 variations in individual models (Fig. 7(b)), are similar to those in the observations in the tropical Indo-Pacific region (Fig. 7(a)). This confirms that most models are able to simulate the relation of the dipole

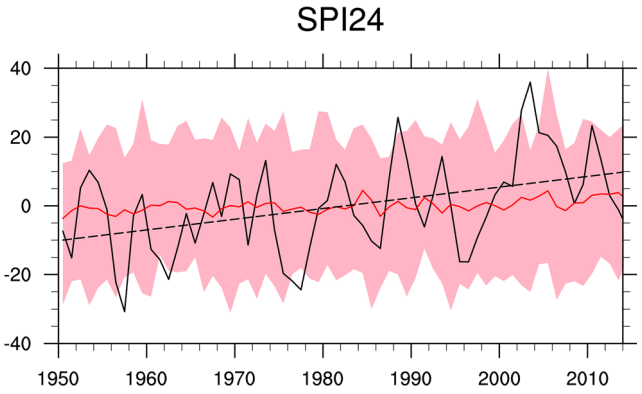

Fig. 6 The first PC time series (black curve) and the corresponding linear trend (dashed line) of the first EOF mode of JJA SPI24 variations based on the CRU precipitation data. The ensemble mean (red curve) and inter-model spread (pink shading) of the first PC time series of the first or second EOF mode of JJA SPI24 variations based on the 42 models

mode of short-term drought variations to the tropical Indo-Pacific SST. In comparison, the model simulated SST anomalies in the tropical Indo-Pacific region shift westward compared to the observations, which is a common feature in climate models (e.g., Collins et al. 2010; Gong et al. 2015). In the North Atlantic region, discrepancy from the observations can be noted in the middle latitudes (Fig. 7(a, b)). In the tropical South Atlantic Ocean, the ensemble mean model SST anomalies are opposite to the observations (Fig. 7(a, b)).

The influence of tropical Indo-Pacific SST anomalies on short-term drought variations is indicated by the accompanying large-scale atmospheric circulation anomaly pattern. Corresponding to the dipole mode of JJA SPI03 variations, anomalous upper-level divergence is observed over the tropical eastern Pacific (Fig. 9(a)). Anomalous upper-level convergence appears over the tropical western Pacific, which indirectly induces anomalous upper-level divergence and anomalous updraft to the north over Central and East Asia. Anomalous upper-level divergence and convergence over the tropical Indo-Pacific shifts westward in the models (Fig. 9(b)) compared to the observations (Fig. 9(a)), which is related to the westward shift of the El Niño–type SST anomalies in the tropical Indo-Pacific region (Fig. 7(a, b)). Consistent with the observations, the model simulates anomalous upper-level divergence and anomalous updraft over Central and East Asia (Fig. 9(a, b)).

We conduct a similar evaluation of the medium-term drought-related SST anomalies corresponding to the dipole mode of interannual JJA SPI09 variations. The observed SST anomalies in DJF and MAM feature an El Niño–type distribution in the tropical Indo-Pacific region (Fig. 10(a, b)). Most of the models capture well the distribution of tropical Indo-Pacific SST anomalies with the PCC values above 0.5 in both DJF and MAM (Fig. 11(a, b)). Exceptions are found in a few models, including BCC-ESM1 and CIESM. Inspection of the SST anomalies in these two models reveals very weak SST anomalies in the tropical Indo-Pacific region (not shown). In the North Atlantic Ocean, the spatial distribution of the SST anomalies in DJF and MAM has a PCC above 0.4 in about half of the models (Fig. 11(c, d)).

The ensemble mean SST anomalies in DJF associated with the dipole mode of JJA SPI09 variations display an El Niño–type distribution in the tropical Indo-Pacific region (Fig. 10(c)), similar to the observations (Fig. 10(a)). Compared to the observations, the SST anomalies tend to shift westward in the tropical Indo-western Pacific region. In the North Atlantic Ocean, the SST anomalies appear weaker in the models than in the observations. The ensemble mean SST anomalies in MAM display a tripole pattern with an eastward displacement in the location of positive SST anomalies in the mid-latitude region (Fig. 10(d)). The above results confirm that most models are able to simulate the relation of the dipole mode of medium-term drought variations to the tropical Indo-Pacific SST.

The accompanying large-scale atmospheric circulation anomaly pattern also confirms the influence of tropical Indo-Pacific SST anomalies on medium-term drought variations. Corresponding to the dipole mode of JJA SPI09 variations, anomalous upper-level divergence and convergence is observed over the tropical eastern and western Pacific, respectively (Fig. 12(a)). Anomalous upper-level divergence and

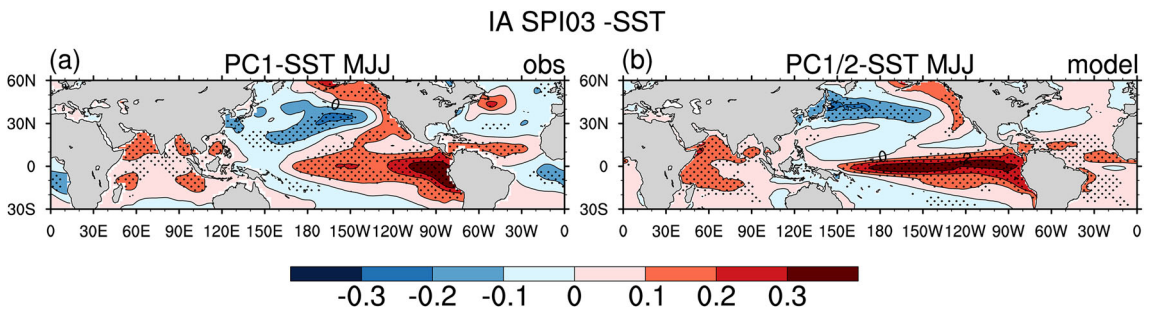

Fig. 7 MJJ SST anomalies (°C) obtained by regression on the PC time series of the dipole EOF mode of interannual component of JJA SPI03 variations for the period 1950–2014 based on (**a**) ERSST5 SST and CRU precipitation data and (**b**) models. Stippling in (**a**) denotes grid points with statistically significant anomalies at the 95% confidence level. Stippling in (**b**) denotes grid points where 80% or more of the 35 models have the same sign SST anomalies

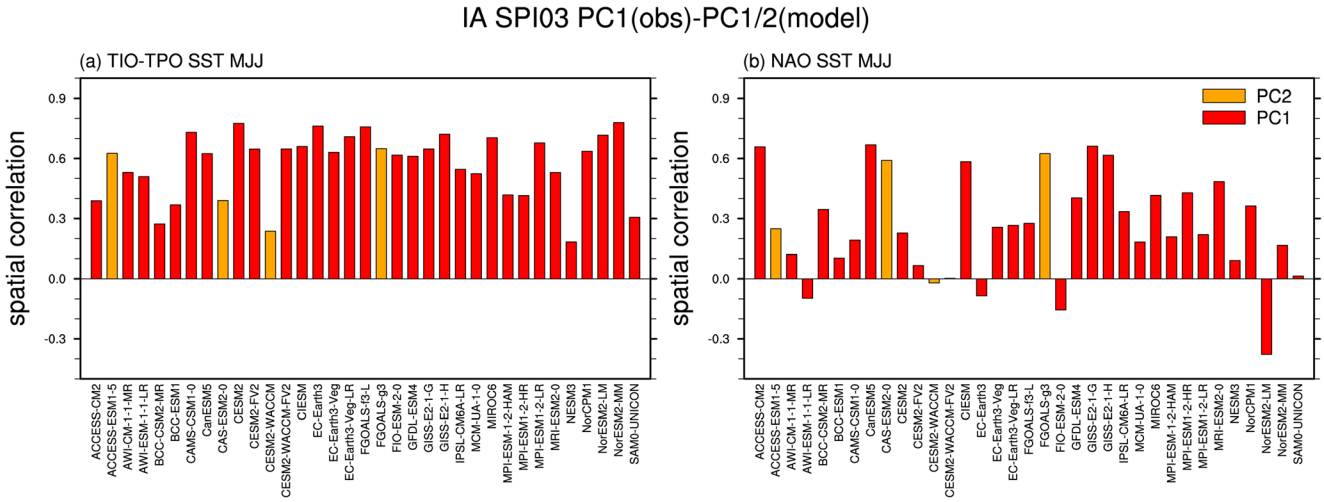

Fig. 8 The spatial pattern correlation coefficient of the MJJ SST anomalies obtained by regression on the dipole EOF mode of interannual component of JJA SPI03 variations between the models and the observations in the (**a**) tropical Indo-Pacific region (30°S–30°N, 40°E–80°W) and (**b**) North Atlantic region (0°–60°N, 70°W–0°)

anomalous updraft are induced over Central and East Asia. The model simulates anomalous upper-level divergence and anomalous updraft over Central and East Asia (Fig. 12(b)). In comparison, anomalous upper-level divergence and convergence over the tropical Indo-Pacific shift westward in the models compared to the observations, which is again attributed to the westward shift of the El Niño–type SST anomalies in the tropical Indo-Pacific region (Fig. 10(a, b)).

The dipole mode of interannual component of JJA SPI24 variations is also linked to an El Niño–type SST anomaly distribution in the tropical Indo-Pacific region and a tripole SST anomaly pattern in the North Atlantic Ocean in the observations (Fig. 13(a, b)). Most of the models reproduce well the tropical Indo-Pacific SST anomalies in JJA(-1) and DJF with the PCC values above 0.5 (Fig. 14(a, b)). In the North Atlantic Ocean, the PCC value is above 0.4 in more than one-third of the models in JJA(-1) and in about half of the models in DJF (Fig. 14(c, d)).

The ensemble mean SST anomalies associated with the dipole mode of the interannual JJA SPI24 variations in the tropical Indo-western Pacific region display a westward shift in the models (Fig. 13(c, d)) compared to the observations. In particular, negative SST anomalies are seen in the region northwest of Australia in JJA(-1) in the models (Fig. 13(c)). Discrepancy from the observations is noted in the distribution of the SST anomalies in the eastern mid-latitude North Atlantic Ocean in JJA(-1) (Fig. 13(c)). In particular, the ACCESS-ESM1-5 displays a distribution of SST anomalies nearly opposite to the observations in the North Atlantic Ocean (not shown) with a PCC value of about −0.4 (Fig. 14(c)). The ensemble mean SST anomalies in the North Atlantic region in DJF are quite similar to the observations (Fig. 13(b, d)). The results indicate that most models are able to simulate the relation of the interannual variation of the dipole mode of long-term drought to the tropical Indo-Pacific and tropical North Atlantic SST.

The dipole mode of interannual component of JJA SPI24 variations is linked to tropical Indo-Pacific SST anomalies through a similar large-scale atmospheric circulation anomaly pattern. Anomalous upper-level divergence and anomalous updraft are induced over Central and East Asia in both the observations and the models (Fig. 15(a, b)). Over the tropical

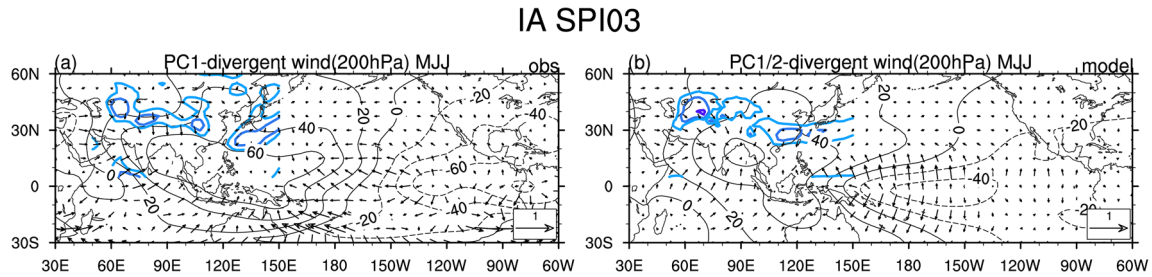

Fig. 9 Anomalies of MJJ divergent wind (vectors, m s^{-1}, scale at the bottom-right corner) and velocity potential (black contours, 10^4 m^2 s^{-1}) at 200 hPa and vertical p-velocities at 500 hPa (blue contours, with negative values of −0.6, −0.3, and -0.1×10^{-2} Pa s^{-1} only in the domain of 5°–60°N and 50°–150°E) obtained by regression on the PC time series of the dipole EOF mode of interannual component of JJA SPI03 variations for the period 1950–2014 based on (**a**) NCEP-NCAR reanalysis and CRU precipitation data and (**b**) models

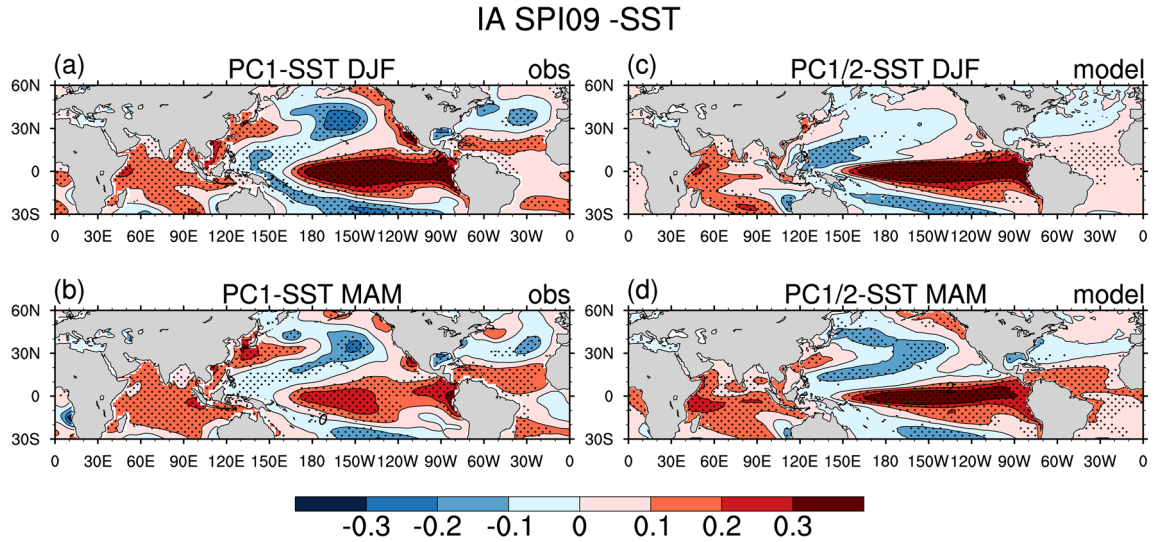

Fig. 10 (**a**, **c**) DJF and (**b**, **d**) MAM SST anomalies (°C) obtained by regression on the PC time series of the dipole EOF mode of interannual component of JJA SPI09 variations for the period 1950–2014 based on (**a**, **b**) ERSST5 SST and CRU precipitation data and (**c**, **d**) models. Stippling in (**a**, **b**) denotes grid points with statistically significant anomalies at the 95% confidence level. Stippling in (**c**, **d**) denotes grid points where 80% or more of the 35 models have the same sign SST anomalies. (**a**)–(**b**) are modified from Zhang and Wu (2021)

Indo-Pacific region, anomalous upper-level divergence and convergence is observed over the eastern and western parts, respectively. Again, the model simulated anomalous upper-level divergence and convergence over the tropical Indo-

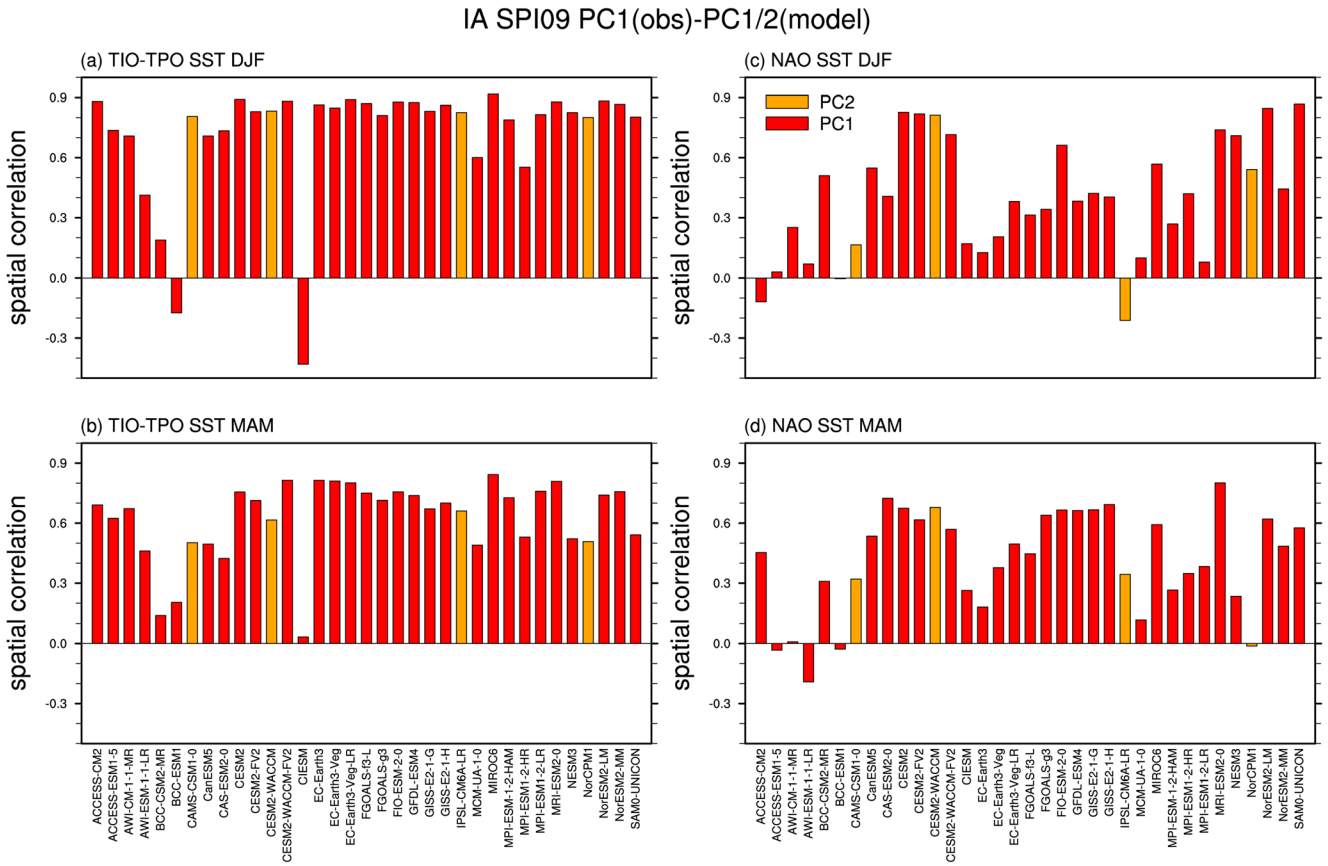

Fig. 11 The spatial pattern correlation coefficient of (**a**, **c**) DJF and (**b**, **d**) MAM SST anomalies obtained by regression on the dipole EOF mode of interannual JJA SPI09 variations between the models and the observations in the (**a**, **b**) tropical Indo-Pacific region (30°S–30°N, 40°E–80°W) and (**c**, **d**) North Atlantic region (0°–60°N, 70°W–0°)

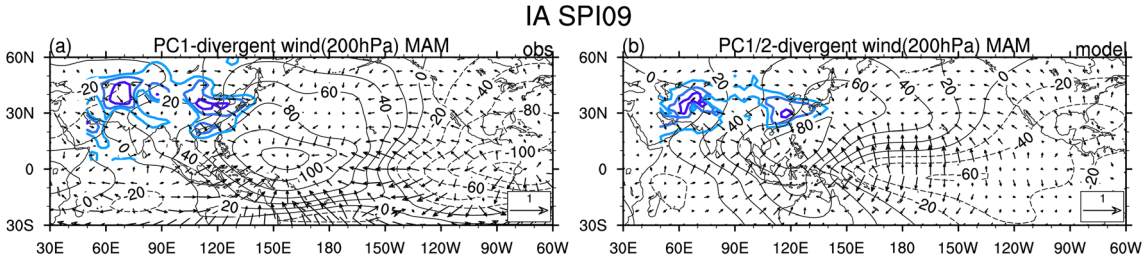

Fig. 12 Anomalies of MAM divergent wind (vectors, m s^{-1}, scale at the bottom-right corner) and velocity potential (black contours, 10^4 m^2 s^{-1}) at 200 hPa and vertical p-velocities at 500 hPa (blue contours, with negative values of −0.6, −0.3, and -0.1×10^{-2} Pa s^{-1} only in the domain of 5°–60°N and 50°–150°E) obtained by regression on the PC time series of the dipole EOF mode of interannual component of JJA SPI09 variations for the period 1950–2014 based on (**a**) NCEP-NCAR reanalysis and CRU precipitation data and (**b**) models. (**a**) is modified from Zhang and Wu (2021)

Pacific shift westward compared to the observations, which is related to the bias in the location of the El Niño–type SST anomalies in the tropical Indo-Pacific region (Fig. 13(a, b)).

5 Summary and discussions

The present study assessed the performance of 42 CMIP6 climate models in simulating the spatial patterns of the Asian summer drought variations based on JJA SPIs during 1950–2014. The short-term, medium-term, and long-term droughts are represented by 3-month, 9-month, and 24-month SPI, respectively. The SST and atmospheric circulation anomalies corresponding to the interannual variations of the leading spatial patterns are assessed for 35 CMIP6 models. The main results of the model performance are summarized in Table 2.

Most of the CMIP6 models can capture the observed leading spatial pattern (Table 2), which is featured by a north-south dipole distribution, of short-term and medium-term drought variations as a leading mode except for a few models (5 models for short-term drought and 7 models for medium-term drought). In those few models, the second mode resembles the observed leading mode. Consistent with the observations, the PC time series of the north-south dipole mode is dominated by interannual variations in all the 42 models, with the explained percent variance more than 75%.

The observed leading spatial pattern of long-term drought variations, featuring a southwest-northeast tripole distribution, is only reproduced in part of the CMIP6 models. The interannual component, interdecadal component, and linear trend contribute to the PC time series of this mode in the models, which agrees with the observations. Further analysis of the long-term drought variations separated into the three components reveals that the interannual variations of long-term drought behave similar to those of short-term and medium-term droughts (Table 2). The discrepancy between the models and observations remains for interdecadal variations and

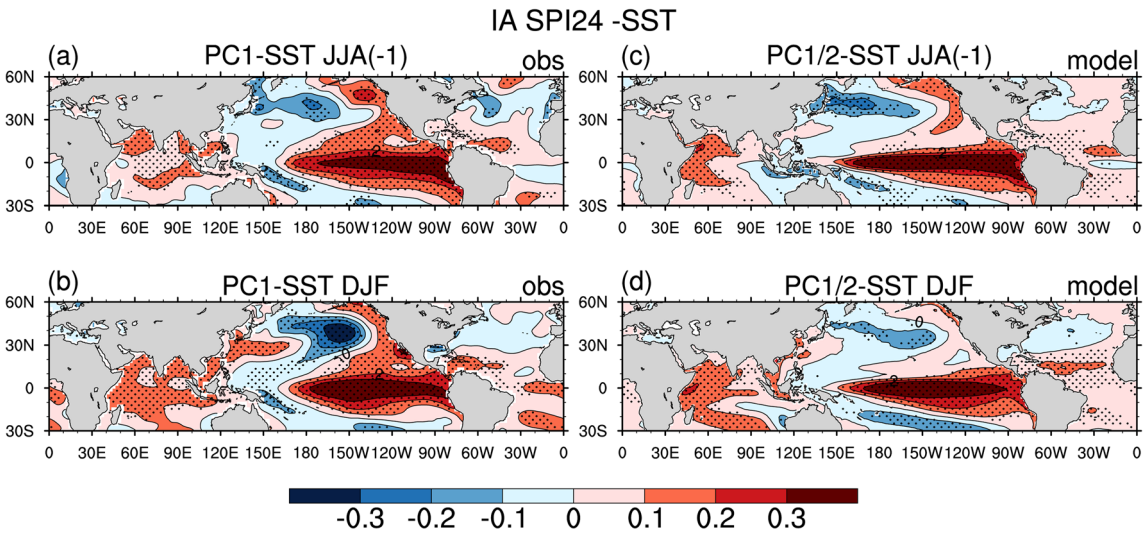

Fig. 13 (**a**, **c**) JJA(-1) and (**b**, **d**) DJF SST anomalies (°C) obtained by regression on the PC time series of the dipole EOF mode of interannual component of JJA SPI24 variations for the period 1950–2014 based on (**a**, **b**) ERSST5 SST and CRU precipitation data and (**c**, **d**) models. Stippling in (**a**, **b**) denotes grid points with statistically significant anomalies at the 95% confidence level. Stippling in (**c**, **d**) denotes grid points where 80% or more of the 35 models have the same sign SST anomalies. (**a**)–(**b**) are modified from Zhang and Wu (2021)

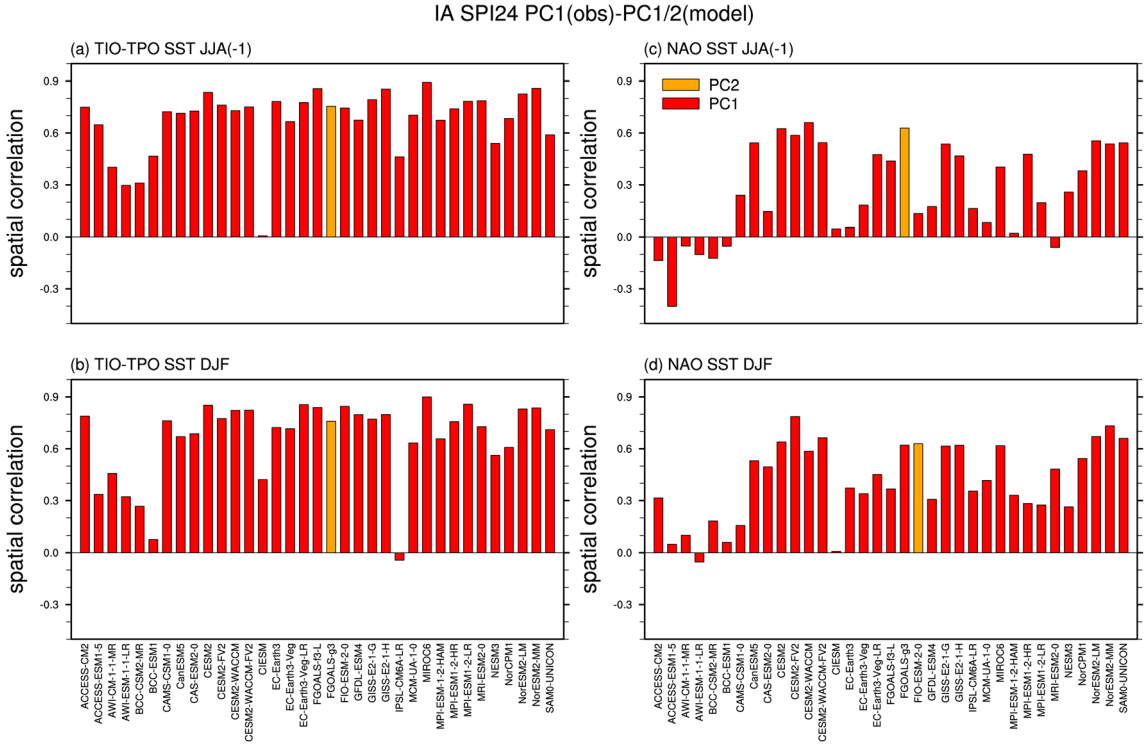

Fig. 14 The spatial pattern correlation coefficient of (**a**, **c**) JJA(-1) and (**b**, **d**) DJF SST anomalies obtained by regression on the dipole EOF mode of interannual component of JJA SPI24 variations between the models and the observations in the (**a**, **b**) tropical Indo-Pacific region (30°S–30°N, 40°E–80°W) and (**c**, **d**) North Atlantic region (0°–60°N, 70°W–0°)

trends of the long-term droughts. This result is consistent with previous studies that found that the CMIP5 models have difficulty to capture the trends of droughts in regional scales (Orlowsky and Seneviratne 2013; Nasrollahi et al. 2015; Ukkola et al. 2018). The reasons for the discrepancy of interdecadal variations of long-term drought between the observations and models remain to be investigated. One plausible reason is the effect of soil moisture anomalies that have persistence, which is important to the maintenance of drought condition (Guan et al. 2009; Wu and Kinter 2009; Cheng et al. 2015; Kong et al. 2019). Our preliminary analysis reveals that the interdecadal soil moisture anomalies have a low spatial correlation coefficient between the observations and models (not shown).

The tropical Indo-Pacific SST anomalies corresponding to the dipole mode of interannual variations of short-term, medium-term, and long-term droughts are characterized by an El Niño–type distribution, with positive SST anomalies in the tropical central-eastern Pacific and tropical Indian Ocean and negative SST anomalies extending northeastward and southeastward from the tropical western Pacific. This SST anomaly pattern is similar to the observations in most of the models for the dipole mode of interannual variations of short-term and medium-term droughts (Table 2). However, there are a few models (BCC-ESM1 and CIESM) that have weak SST anomalies in the tropical Indo-Pacific region corresponding to the dipole mode of interannual variations of medium-term

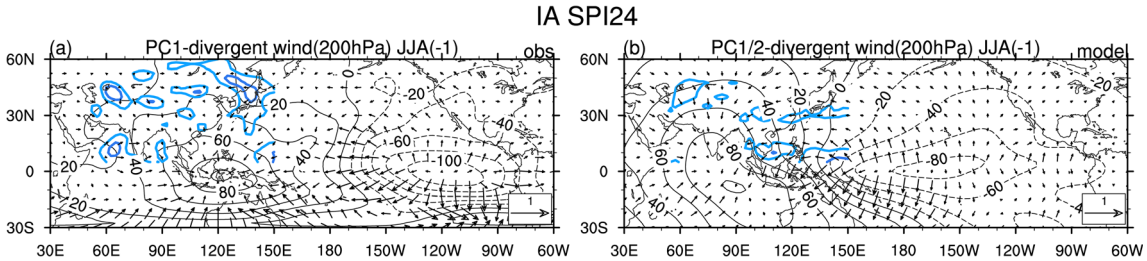

Fig. 15 Anomalies of JJA(-1) divergent wind (vectors, m s^{-1}, scale at the bottom-right corner) and velocity potential (black contours, 10^4 m^2 s^{-1}) at 200 hPa and vertical p-velocities at 500 hPa (blue contours, with negative values of −0.6, −0.3, and -0.1×10^{-2} Pa s^{-1} only in the domain of 5°–60°N and 50°–150°E) obtained by regression on the PC time series of the dipole EOF mode of interannual component of JJA SPI24 variations for the period 1950–2014 based on (**a**) NCEP-NCAR reanalysis and CRU precipitation data and (**b**) models. (**a**) is modified from Zhang and Wu (2021)

Table 2 A summary of model performance of interannual variations of short-term, medium-term, and long-term droughts in JJA over Asia against the observations (obs). The ratio within parentheses denotes that the number of models out of total models in which the pattern correlation coefficient (PCC) with the corresponding observations reaches 0.5 in the domain of 5°–60°N and 50°–150°E for the spatial pattern of drought variations in JJA, 0.4 in the domain of 30°S–30°N and 40°E–80°W for the tropical Indo-Pacific SST anomalies, and 0.4 in the domain of 0°–60°N and 70°W–0° for the North Atlantic SST anomalies in MJJ (SPI03), DJF (SPI09), and DJF (SPI24), respectively

		Short-term drought	Medium-term drought	Long-term drought		
				Interannual	Interdecadal	Trend
Spatial pattern	Obs	Dipole	Dipole	Dipole	Tripole	Scattered
	Model	Dipole (42/42)	Dipole (37/42)	Dipole (39/42)	Weak	Weak
Indo-Pacific SST anomaly	Obs	El Niño	El Niño	El Niño		
	Model	El Niño (28/35)	El Niño (32/35)	El Niño (30/35)		
North Atlantic SST anomaly	Obs	Tripole	Tripole	Tripole		
	Model	Tripole (11/35)	Tripole (18/35)	Tripole (18/35)		

drought. Most of the models also capture the El Niño–type distribution of SST anomalies in the tropical Indo-Pacific region corresponding to the dipole mode of interannual variations of long-term drought (Table 2).

The North Atlantic SST anomalies corresponding to the dipole mode of interannual variations of droughts display a tripole pattern in the observations, with positive SST anomalies in the tropics and middle latitudes and negative SST anomalies in the subtropics. Only about one-third to half of the models capture the observed North Atlantic tripole SST anomaly pattern (Table 2). More models simulate the tripole SST anomaly pattern in the North Atlantic Ocean in DJF than in JJA(-1) corresponding to the dipole mode of interannual variations of long-term droughts.

The link of the dipole mode of drought variations with the tropical Indo-Pacific SST anomalies is related to a large-scale atmospheric circulation anomaly pattern with a west-east contrast of anomalous upper-level divergence and convergence over the tropical Indo-Pacific region. In comparison, the above pattern shifts westward in the models in association with a westward extension of the tropical Indo-Pacific SST anomalies. Anomalous upper-level divergence and anomalous updraft are induced over Central and East Asia in both the observations and models.

The present evaluation of spatial patterns of Asian summer drought variations in the models is only based on the SPI. Previous studies noted that the characteristics and changes of droughts may depend upon the index used to measure droughts (Orlowsky and Seneviratne 2013; Nasrollahi et al. 2015; Ukkola et al. 2018). Further evaluations using other drought indices are needed to provide a comprehensive understanding of the drought changes in the models compared to the observations.

Our evaluation illustrates that most models are able to capture the leading spatial patterns of short-term and medium-term drought variations and interannual component of long-term drought variations as well as their associations with the tropical Indo-Pacific SST anomalies. This is attributed to the ability of most models to capture the large-scale atmospheric circulation anomaly pattern induced by the tropical Indo-Pacific SST anomalies. Thus, it is suitable to investigate historical and future changes and associated mechanisms of interannual variations of meteorological drought using models. However, most models have difficulty to reproduce the spatial patterns of interdecadal variations and long-term changes of meteorological droughts. This suggests that current models are not suitable for projection of future changes in long-term meteorological droughts.

Regarding the spatial patterns of droughts, some of the models display notable discrepancies from the observations and other models. For example, the observed dipole pattern of short-term and medium-term drought variations shows up as the second EOF mode in a few models. Regarding the distribution of SST anomalies corresponding to the dipole mode of drought variations, some models fail to simulate the observed El Niño–type SST anomaly pattern in the tropical Indo-Pacific region and the tripole SST anomaly pattern in the North Atlantic region. Further work is needed to explore the plausible reasons for these discrepancies between models and the observations.

Acknowledgements Comments of two anonymous reviewers are appreciated. The CRU precipitation data were obtained at https://crudata.uea.ac.uk/cru/data/precip/. The ERSST data were obtained at https://www.

ncdc.noaa.gov/. CMIP6 model data were obtained from https://esgf-node.llnl.gov/search/cmip6/.

Author contribution YZ prepared the data, performed the analysis, plotted the figures, and drafted the paper. RW provided the idea and guided the analysis. Both contributed to the revising and editing of the paper.

Funding This study is supported by the National Natural Science Foundation of China grants (41721004 and 41775080).

Availability of data and materials Data used in the analysis are available on public websites.

Code availability Not applicable

Declarations

Ethics approval Not applicable

Consent to participate Not applicable

Consent for publication Both authors agree the submission and publication of the paper.

Competing interests The authors declare no competing interests.

References

Ault TR, Cole JE, George SS (2012) The amplitude of decadal to multidecadal variability in precipitation simulated by state-of-the-art climate models. Geophys Res Lett 39:L21705. https://doi.org/10.1029/2012GL053424

Barriopedro D, Gouveia CM, Trigo RM, Wang L (2012) The 2009/10 drought in China: possible causes and impacts on vegetation. J Hydrometeorol 13:1251–1267. https://doi.org/10.1175/JHM-D-11-074.1

Burke EJ, Brown SJ (2008) Evaluating uncertainties in the projection of future drought. J Hydrometeorol 9:292–299. https://doi.org/10.1175/2007JHM929.1

Cheng S, Guan X, Huang J, Ji F, Guo R (2015) Long-term trend and variability of soil moisture. J Geophys Res Atmos 120:8658–8670. https://doi.org/10.1002/2015JD023206

Collins M, An SI, Cao W, Ganachaud A, Guilyardi E, Jin FF, Jocum M, Lengaigne M, Poer S, Timmermann A, Vecchi G, Wittenberg A (2010) The impact of global warming on the tropical Pacific Ocean and El Niño. Nat Geosci 3:391–397. https://doi.org/10.1038/ngeo868

Dai A (2011) Drought under global warming: a review. Wiley Interdiscip Rev Clim Chang 2:45–65. https://doi.org/10.1002/wcc.81

Dai A (2013) Increasing drought under global warming in observations and models. Nat Clim Chang 3:52–58. https://doi.org/10.1038/nclimate1633

Damberg L, AghaKouchak A (2014) Global trends and patterns of droughts from space. Theor Appl Climatol 117(3):441–448. https://doi.org/10.1007/s00704-013-1019-5

Eyring V, Bony S, Meehl GA, Senior CA, Stevens B, Stouffer RJ, Taylor KE (2016) Overview of the Coupled Model Intercomparison Project Phase 6 (CMIP6) experimental design and organization. Geosci Model Dev 9:1937–1958. https://doi.org/10.5194/gmd-9-1937-2016

Gong H, Wang L, Chen W, Nath D, Huang G, Tao W (2015) Diverse influences of ENSO on the East Asian–western Pacific winter climate tied to different ENSO properties in CMIP5 models. J Clim 28:2187–2202. https://doi.org/10.1175/JCLI-D-14-00405.1

Guan X, Huang J, Guo N, Bi J, Wang G (2009) Variability of soil moisture and its relationship with surface albedo and soil thermal parameters over the Loess Plateau. Adv Atmos Sci 26:692–700. https://doi.org/10.1007/s00376-009-8198-0.1

Guan X, Huang J, Guo R, Lin P (2015a) The role of dynamically induced variability in the recent warming trend slowdown over the Northern Hemisphere. Sci Rep 5:12669. https://doi.org/10.1038/srep12669

Guan X, Huang J, Guo R, Yu H, Lin P, Zhang Y (2015b) Role of radiatively forced temperature changes in enhanced semi-arid warming in the cold season over east Asia. Atmos Chem Phys 15:13777–13786. https://doi.org/10.5194/acp-15-13777-2015

Guan X, Huang J, Guo R (2017) Changes in aridity in response to the global warming hiatus. J Meteorol Res 31:117–125. https://doi.org/10.1007/s13351-017-6038-1

Guan X, Ma J, Huang J, Huang R, Zhang L, Ma Z (2019) Impact of oceans on climate change in drylands. Sci China Earth Sci 62:891–908. https://doi.org/10.1007/s11430-018-9317-8

Harris I, Jones PD, Osborn TJ, Lister DH (2014) Updated high-resolution grids of monthly climatic observations–the CRU TS3.10 Dataset. Int J Climatol 34:623–642. https://doi.org/10.1002/joc.3711

Hayes M, Svoboda M, Wall N, Widhalm M (2011) The Lincoln declaration on drought indices: universal meteorological drought index recommended. Bull Am Meteorol Soc 92(4):485–488

Huang J, Zhang W, Zuo J, Bi J, Shi J, Wang X, Chang Z, Huang Z, Yang S, Zhang B, Wang G, Feng G, Yuan J, Zhang L, Zuo H, Wang S, Fu C, Jifan C (2008) An overview of the semi-arid climate and environment research observatory over the Loess Plateau. Adv Atmos Sci 25:906–921. https://doi.org/10.1007/s00376-008-0906-7

Huang J, Guan X, Ji F (2012) Enhanced cold-season warming in semi-arid regions. Atmos Chem Phys 12:5391–5398. https://doi.org/10.5194/acp-12-5391-2012

Huang Y, Gerber S, Huang T, Lichstein JW (2016) Evaluating the drought response of CMIP5 models using global gross primary productivity, leaf area, precipitation, and soil moisture data. Glob Biogeochem Cycles 30:1827–1846. https://doi.org/10.1002/2016GB005480

Huang B, Peter WT, Banzon VF, Boyer T, Chepurin G, Lawrimore JH, Menne MJ, Smith TM, Vose RS, Zhang H-M (2017a) Extended Reconstructed Sea Surface Temperature version 5 (ERSSTv5). Upgrades, validations, and intercomparisons. J Clim 30:8179–8205. https://doi.org/10.1175/JCLI-D-16-0836.1

Huang J, Yu H, Dai A, Wei Y, Kang L (2017b) Drylands face potential threat under 2°C global warming target. Nat Clim Chang 7:417–422. https://doi.org/10.1038/nclimate3275

Kim DW, Byun HR (2009) Future pattern of Asian drought under global warming scenario. Theor Appl Climatol 98:137–150. https://doi.org/10.1007/s00704-008-0100-y

Kong X, Guan X, Cao C, Zhang T, Shen L, Gan Z, Ma J, Huang H (2019) Decadal Change in soil moisture over East Asia in response to a decade-long warming hiatus. J Geophys Res Atmos 124:8619–8630. https://doi.org/10.1029/2019JD030294

Lehner F, Coats S, Stocker TF, Pendergrass AG, Sanderson BM, Raible CC, Smerdon JE (2017) Projected drought risk in 1.5°C and 2°C warmer climates. Geophys Res Lett 44:7419–7428. https://doi.org/10.1002/2017GL074117

Lewis S, Brando P, Phillips O, van der Heijden G, Nepstad D (2011) The 2010 Amazon drought. Science 331:554–554

Lopes-Moreno JI, Vicente-Serrano SM (2008) Positive and negative phases of the wintertime North Atlantic Oscillation and drought occurrence over Europe: a multitemporal-scale approach. J Clim 21:1220–1243

McGrath GS, Sadler R, Fleming K, Tregoning P, Hinz C, Veneklaas EJ (2012) Tropical cyclones and the ecohydrology of Australia's recent continental-scale drought. Geophys Res Lett 39:L03404. https://doi.org/10.1029/2011GL050263

McKee T, Doesken N, Kleist J (1993) The relationship of drought frequency and duration to time scales. Eighth Conference on Applied Climatology, Am Meteorol Soc, Anaheim, pp 179–184

Nasrollahi N, AghaKouchak A, Cheng L, Damberg L, Phillips TJ, Miao C, Hsu K, Sorooshian S (2015) How well do CMIP5 climate simulations replicate historical trends and patterns of meteorological droughts? Water Resour Res 51:2847–2864. https://doi.org/10.1002/2014WR016318

Orlowsky B, Seneviratne SI (2012) Global changes in extreme events: Regional and seasonal dimension. Clim Chang 110:669–696. https://doi.org/10.1007/s10584-011-0122-9

Orlowsky B, Seneviratne SI (2013) Elusive drought: uncertainty in observed trends and short- and long-term CMIP5 projections. Hydrol Earth Syst Sci 17:1765–1781. https://doi.org/10.5194/hess-17-1765-2013

Peterson T, Stott P, Herring S (2012) Explaining extreme events of 2011 from a climate perspective. Bull Am Meteorol Soc 93:1041–1067

Prudhomme C, Giuntoli I, Robinson EL, Clark DB, Arnell NW, Dankers R, Fekete BM, Franssen W, Gerten D, Gosling SN, Hagemann S, Hannah DM, Kim H, Masaki Y, Satoh Y, Stacke T, Wada Y, Wisser D (2014) Hydrological droughts in the 21st century, hotspots and uncertainties from a global multimodel ensemble experiment. Proc Natl Acad Sci U S A 111(9):3262–3267. https://doi.org/10.1073/pnas.1222473110

Sheffield J, Wood EF (2008) Projected changes in drought occurrence under future global warming from multi-model, multi-scenario, IPCC AR4 simulations. Clim Dyn 31:79–105. https://doi.org/10.1007/s00382-007-0340-z

Sheffield J, Wood E, Roderick M (2012) Little change in global drought over the past 60 years. Nature 491(7424):435–438

Su B, Huang J, Fischer T, Wang Y, Kundzewicz ZW, Zhai J, Sun H, Wang A, Zeng X, Wang G, Tao H, Gemmer M, Li X, Jiang T (2018) Drought losses in China might double between the 1.5°C and 2.0°C warming. Proc Natl Acad Sci U S A 115:10600–10605. https://doi.org/10.1073/pnas.1802129115

Taylor IH, Burke E, McColl L, Falloon P, Harris GR, McNeall D (2012) Contributions to uncertainty in projections of future drought under climate change scenarios. Hydrol Earth Syst Sci Discuss 9(11):12613–12653. https://doi.org/10.5194/hessd-9-12613-2012

Touma D, Ashfaq M, Nayak MA, Kao SC, Diffenbaugh NS (2015) A multi-model and multiindex evaluation of drought characteristics in the 21st century. J Hydrometeorol 526:196–207. https://doi.org/10.1016/j.jhydrol.2014.12.011

Trenberth KE, Dai A, van der Schrier G, Jones PD, Barichivich J, Briffa KR, Sheffield J (2014) Global warming and changes in drought. Nat Clim Chang 4(1):17–22

Ukkola AM, Pitman AJ, De Kauwe MG, Abramowitz G, Herger N, Evans JP, Decker M (2018) Evaluating CMIP5 model agreement for multiple drought metrics. J Hydrometeorol 19(6):969–988. https://doi.org/10.1175/JHM-D-17-0099.1

White RP, Nackoney J (2003) Drylands, people, and ecosystem goods and services: a web-based geospatial analysis. World Resources Institute. http://pdf.wri.org/drylands.pdf. Accessed 30 Jan 2012

Wilhite D (2000) Drought as a natural hazard: concepts and definitions. In: Wihite D (ed) Drought: A Global Assessment. Routledge, London, pp 3–18

Wu R, Kinter JL (2009) Analysis of the relationship of U. S. droughts with SST and soil moisture: distinguishing the time scale of droughts. J Clim 22:4520–4538. https://doi.org/10.1175/2009JCLI2841.1

Wu C-H, Yeh PJ-F, Chen Y-Y, Hu BX, Huang G (2020) Future precipitation-driven meteorological drought changes in the CMIP5 multimodel ensembles under 1.5 °C and 2 °C global warming. J Hydrometeorol 21(9):2177–2196. https://doi.org/10.1175/JHM-D-19-0299.1

Zargar A, Sadiq R, Naser B, Khan FI (2011) A review of drought. Environ Rev 19:333–349

Zhang L, Zhou T (2015) Drought over East Asia: a review. J Clim 28:3375–3399. https://doi.org/10.1175/JCLI-D-14-00259.1

Zhang Y, Wu R (2021) Asian meteorological droughts on three time scales and different roles of SST and soil moisture. Int J Climatol. https://doi.org/10.1002/joc.7617

Zhang Y, Guan X, Yu H, Xie Y, Jin H (2017) Contribution of radiative factors to enhanced drylands warming over East Asia. J Geophys Res Atmos 122:7723–7736. https://doi.org/10.1002/2017JD026506

Zhao T, Dai A (2015) The magnitude and causes of global drought changes in the twenty-first century under a low moderate missions scenario. J Clim 28:4490–4512. https://doi.org/10.1175/JCLI-D-14-00363.1